J Mater Sci (2006) 41:6237–6244
DOI 10.1007/s10853-006-0720-5

Impact–fatigue behaviour of unidirectional carbon fibre reinforced polyetherimide (PEI) composites

Tamer Sınmazçelik · A. Armağan Arıcı · Volkan Günay

Received: 22 April 2004 / Accepted: 21 October 2005 / Published online: 12 August 2006

Abstract Impact fatigue properties of unidirectional carbon fibre-reinforced polyetherimide (PEI) composites was evaluated by subjecting standard izod impact samples to low velocity impact loading at energy levels ranging 0.16–1.08 J by using Ceast Model Resil 25, a pendulum type instrumented impact test system. The effect of the previous low velocity impacts on the impact properties of the laminates was investigated. On the other hand materials were subjected to repeated low velocity impact tests up to fracture. Results of repeated impact study are reported in terms of peak load, absorbed energy and number of impacts. Fractographic analysis revealed the fracture by primary debonding, with fibre breakage and pullout in the tensile zone, but a shear fracture of fibre bundles in the compressive zone of the specimen.

Introduction

Although continuous fibre reinforced composite laminates have advantages such as high specific strength and stiffness, and high chemical resistance, they are susceptible to damage caused by various loadings that include static loading, low energy impact loading during manufacture and in service. Polymer composites have excellent mechanical properties over conventional metallic materials; their use in advanced technological applications has been limited due to their poor translaminar properties. Failures of fibre reinforced polymer composites under single and repeated impacts analogous to fatigue are of concern to the designers and users in military and aerospace structures. Catastrophic crack propagation due to the impact loading conditions in various composite structures is of serious concern. Crack initiation and propagation can occur in composite materials due to various scenarios like low velocity, high strain rate and ballistic impacts. Such impacts may occur during fabrication, normal maintenance operations or during service conditions. Such damages are not detectable to the naked eye (the damage being in a subsurface region or being too small to be visible to the naked eye), which adds to the critical nature of low velocity impact damage. The material failure, which is induced by repeated impact loading, is major concern because there is significant loss of stiffness and compressive strength of the composite material. On the other hand, during routine maintenance activities and during operation, composite components may be subjected to repeated impact at localized sites. The resultant damage may seriously impair the subsequent mechanical performance of the composites. Delamination and debonding are the major failure modes for composites as a result of impact loading [1]. It was reported that delamination effects under impact cause severe degradation of tensile and compressive properties [2]. Thus the suitability of a composite under impact is determined not only by the usual design parameters but also by its impact energy absorbing properties.

T. Sınmazçelik (✉) · A. Armağan Arıcı
Mechanical Engineering Department, Kocaeli University, Veziroğlu Campus, 41040 İzmit, Turkey
e-mail: tamersc@yahoo.com

V. Günay · T. Sınmazçelik
Materials Institute, TUBITAK-Marmara Research Centre, P.O.Box 21, 41470 Gebze, Turkey

Impact response is generally governed by parameters like impact velocity, type of fibres and matrix used, volume fraction of fibres and interfacial bonding [3]. Fibre pullout and shear failure, matrix cracking, debonding and delamination are some of the various types of damages that have been reported [4–6].

The residual strength at various energy levels following impact, or post-impact testing, are some of the recent research topics in the literature [7]. Cantwell et al. [8] examined the fatigue residual strength of carbon/epoxy composites subject to impact. However, few authors investigated repeated impacts on composites [9–13]. Lhymn [14, 15] determined the number of impacts to failure of a short E-glass fibre/PPS composite for a given energy level and developed a theoretical lifetime analysis. The residual tensile and compressive strengths of selected carbon fibre reinforced epoxy resin composites subjected to repeated impacts were measured by Wyrick and Adams [9]. Rotem [16] showed that, when a low-energy impact was exerted on a laminate, invisible damage occurred as a result of the contact stresses between the impactor and the laminate. The damage zone grew and caused a certain amount of strength and modulus reduction. Tamuzs and co-workers [17] monitored the variation in the rigidity of glass fibre reinforced plastics during tensile impact fatigue testing. Jang and co-workers [18] reported the failure mechanisms of continuous fibre reinforced epoxy and PPS composites under repeated impact fatigue testing and concluded that the impact fatigue test had been found to be a convenient method for assessing the damage tolerance of both thermoplastic and thermoset composites.

The objective of this study is to investigate the effect of the previous low velocity pre-impacts on the impact properties of the laminates and to understand the lifetime of the material, which is subjected to the repeated impacts at different energy levels. Results of repeated impact study were reported in terms of peak load, absorbed energy and number of impacts. Fractographic investigations were carried out to analyse the crack growth and the failure mechanism during the impact fatigue loading.

Experimental procedures

Unidirectional carbon fibre reinforced polyetherimide (PEI) composites were kindly supplied by Ten Cate Advanced Composites (Nijverdal/Netherlands) in the form of hot pressed plaques. Fibre volume content is 60%. Plaques manufactured from 14 plies with a ply thickness of 0.14 mm and the area weight of ply is 222 g/m^2. The commercial code of the laminate is CD5150.

Impact tests were performed on an instrumented Ceast pendulum type tester (Resil 25) and test samples were prepared according to ISO 180 standards. Un-notched samples were used with the dimensions of $10 \times 2 \times 65$ mm. Preliminary experiments were performed in order to find the appropriate falling angle, which was chosen as 50^o in order to remove the inertial oscillations in the contact load between striker and sample. The strike range of the hammer, at 50^o falling angle (Izod hammer), was 1.08 kN. Hammer length and mass were 0.327 m and 2.508 kg, respectively. Sampling time was 8 μs. Impact velocity was 1.51 m/s, and maximum available energy was 2.87 J. Before discussing these results it is important to understand the approach used in the analysis of force-time curves, which is critical in determining the impact characteristics of materials. Upon impact of the pendulum, the force rises sharply to a maximum value (F_{max}) and then gradually decays to zero due to catastrophic failure. The total area under the force–time curve gives the impact energy for the system (E_{max}). These curves can be divided into two regions. The first region is the crack initiation and the second is the crack propagation regions. The areas under each region give the energy for these processes, which are defined as energy for crack initiation (E_i) and energy for crack propagation (E_p). The spikes in the first region are due to inertial oscillations of the sample.

Fractured surfaces of the impact test samples were examined by scanning electron microscopy, (SEM), using a JOEL JSM-6335F field emission scanning microscope.

Results and discussions

The first group of experiments were carried out by placing Izod samples into the instrumented impact tester as illustrated in Fig. 1 and struck with the pendulum hammer, with small impact energies. These impact energies were not big enough to fracture the samples but they were big enough to cause elasto-plastic deformation in the material. The impact energies of Izod hammer were chosen as 0.03, 0.12, 0.27, 0.35, 0.39, 0.49, 0.75, 1.08 and 1.45 J. With the same sequence of the impact energy of hammer, the striking velocity changes as 0.16, 0.31, 0.47, 0.53, 0.56, 0.62, 0.78, 0.93 and 1.08 m/sec. The hammer struck each sample only once. The samples were preserved from additional strikes of the hammer. These samples were called ''pre-impacted samples'' and their force–time curves are

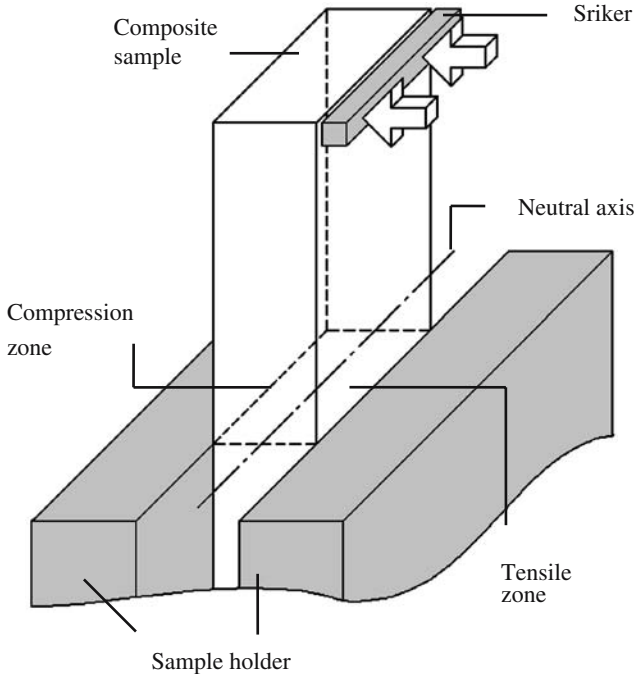

Fig. 1 Schematic illustration of instrumented impact tester and sample geometry

illustrated in Fig. 2. Finally, all of the previously impacted samples were put into the impact tester and fractured by the Izod hammer, with an impact energy of 2.87 J. This impact was called the ''final impact''. Table 1 provides the numerical results after the final impact. The residual impact properties of composites subjected to repeated impacts were also measured by similar methods by Roy et al [6], Wyrick and Adams [9] and by Rotem [16].

It was observed that there was not crack initiation as a result of the previous impacts (pre-impact) up to impact energy of 0.39 J. Remarkable crack initiation and propagation was observed at the impact energy of 1.45 J, which was the highest impact energy used for previous impacts of the samples. Previous impacts caused deformations at the sub surface of the material. Increases in the impact energy up to 1.45 J caused higher F_{max} and E_{max} values. Figure 3 illustrates the F_{max} values of both previous and final impacts. It was observed that F_{max} values of previous impacts are proportional with the impact energy of the hammer. On the other hand at Fig. 3, the curve displayed three regions after the final impacts as shown by Roy et al. [6]. At first region F_{max} values as a result of final impacts remains nearly constant up to impact energy of 0.39 J. In region 1, the previous impacts here were not sufficient to enlarge the microcracks and debonding to cause a fracture where also observed by previous studies [6, 15, 18, 19]. The 2nd region can be called as transition zone, where the F_{max} values showed sharp decrease. This region is started at 0.39 J and ended at 0.75 J of impact energy. Because of the crack initiations occur at 0.39 J after previous impacts, during the final impact samples were fractured with lower F_{max} values. In 2nd region as a result of previous impacts the formations of microcracks in the matrix, which

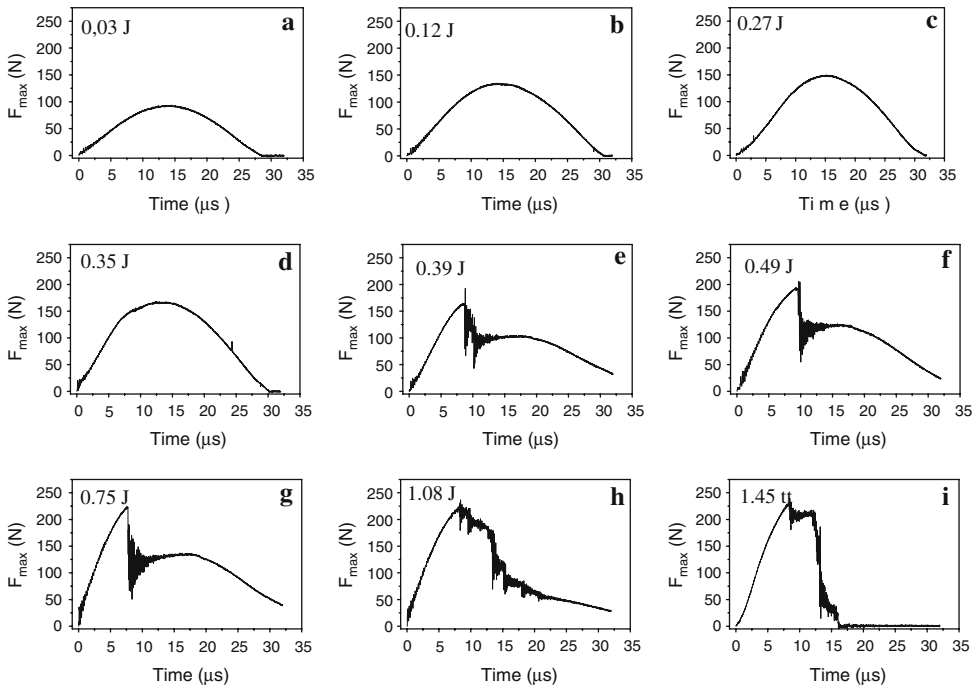

Fig. 2 Impact response of samples subjected to previous impacts at different impact energies of hammer

Table 1 Numerical results of preliminary and final impact test results

Preliminary impact results						Final impact results					
Falling angle (◦)	Impact energy (J)	F_{max} (N)	E_i (J)	E_p (J)	E_{max} (J)	Falling angle (◦)	Impact energy (J)	F_{max} (N)	E_i (J)	E_p (J)	E_{max} (J)
0	0	-	-	-	-	50	2.87	208	0.492	0.649	1.141
5	0.03	101	-	-	0.032	50	2.87	208	0.362	0.656	1.018
10	0.12	142	-	-	0.121	50	2.87	236	0.424	0.615	1.039
15	0.27	172	-	-	0.277	50	2.87	196	0.346	0.523	869
17	0.35	165	-	-	0.352	50	2.87	196	0.546	0.524	1.070
18	0.39	189	0.287	0.106	0.393	50	2.87	210	0.454	0.444	0.898
20	0.49	202	0.300	0.181	0.481	50	2.87	130	0.494	0.411	0.905
25	0.75	205	0.356	0.403	0.759	50	2.87	152	0.523	0.177	0.700
30	1.08	248	0.401	0.596	0.997	50	2.87	103	0.391	0.164	0.555
35	1.45	213	0.244	0.799	1.043	50	2.87	103	0.369	0.368	0.737

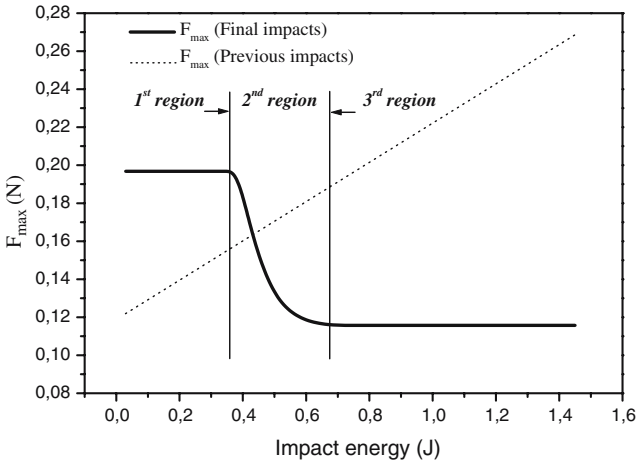

Fig. 3 F_{max} results after previous and final impacts

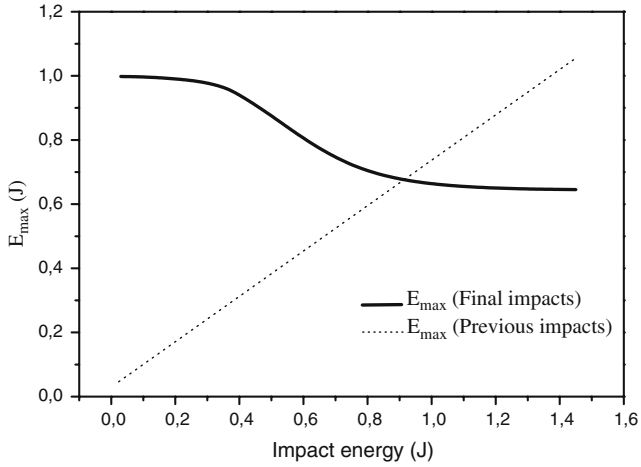

Fig. 4 E_{max} results after previous and final impacts

enlarged by coalescence [6] with the spread of the debonded zones, became predominant. The sharp decreases in F_{max} values ended at 0.75 J. After this impact energy of hammer, the 3rd region is started. It is observed that F_{max} values didn't show any difference between 0.75 J and 1.45 J. After the previous impacts of 1.45 J, materials have a remarkable failure and fractured after the final impact with a very small energy. As seen in Fig. 4, the relationship of impact energy of the hammer show a great similarity to F_{max} results. It is possible to observe three different regions in Fig. 4. But the 2nd region didn't have sharp decrease as in Fig. 3. It was observed that both E_i and E_p values were increasing proportional to the impact energy of hammer. As seen in Table 1 as a result of previous impacts both E_i and E_p values increases by the impact energy after 0.39 J. Even at very small impact energy of 0.03 J previous impact has noteworthy changes at impact performance of the materials. Both E_i and E_{max} values decreases at final impacts of previously impacted samples at 0.03 J. Table 1 provides that there is a remarkable decreasing at E_p values at final impact samples, which were previously impacted with 0.39 J and higher impact energies. Previously impacted eight samples with 1.45 J were fractured at final impact with a very small energy reading which tester couldn't measure. The numerical mean value results of other two samples are presented in Table 1.

Second group of experiment were carried out to investigate the impact–fatigue behaviour of the materials. Materials are subjected to repeated impact loading with various impact energy of izod hammer up to fracture. Impact–fatigue tests were performed with the hammer impact energies of 0.27, 0.35, 0.39, 0.44, 0.49, 0.75, 1.08 and 1.45 J. Very similar to previous studies [1, 6], as seen in Fig. 5, decreasing in impact energies results in increasing number of impacts up to break. Figure 5 shows the S–N type impact fatigue curve of the composite material. Figure 6 provides force–time (F–t) curves of impact–fatigue experiments, which are performed with the impact energy of 0.35 J. This sample is fractured at 422nd impact. It should be noted that, no crack initiation was observed at first impact at 0.35 J. Although without having a crack

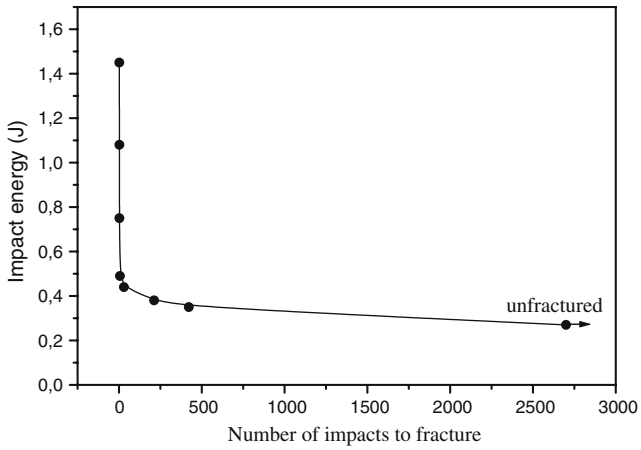

Fig. 5 The relationship between the impact energy of hammer and number of impacts to fracture

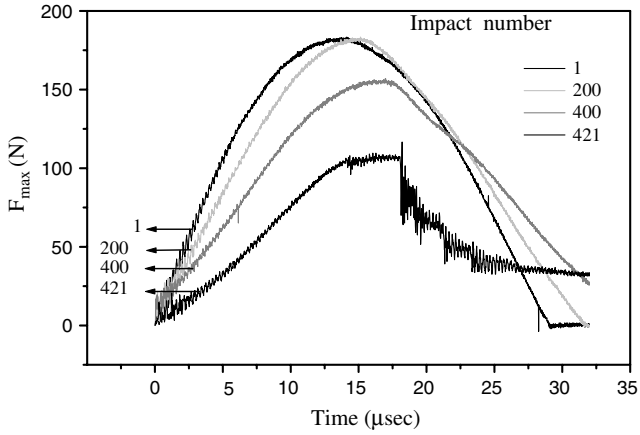

Fig. 6 Impact response of samples subjected to repeated impact loading with an impact energy of 0.35 J

initiation, sample was fractured after a typical impact–fatigue failure. As provided in Fig. 6 the modulus and the F_{max} values are decreasing with increasing impact number. At 421st impact the sample has a remarkable failure and it was fractured at 422nd impact but the machine couldn't measure the fracture energy. During the impact–fatigue experiments at the impact energy of 0.27 J, no crack initiation was observed even after 2801st impact. The experiments were stopped, because as seen in Fig. 5 that the relationship between the impact energy and impact number is determined after impact–fatigue tests and 0.27 J seems as an asymptote of this curve.

By using the capabilities of instrumented impact testing, it is possible to understand the failure history of impacted samples. It is also possible to investigate how the material response to the loading when the crack initiation is started during the impact–fatigue testing. Especially the characteristic changes at crack initiation and propagation gives us comprehensive descriptions about the failure. On the other hand, beside the numerical results microscopical investigations give us details about the failure characteristics and crack propagation. SEM investigations were carried out to understand the crack initiation and propagation mechanisms.

Figure 7 and 8 exhibited a remarkable difference between the single-impact fractured and impact–fatigue fractured specimens. As seen in Fig. 7 the ratio of tensile/compression area is approximately 1.4 at fractured sample, which was fractured by single impact with 2.87 J. On the other hand this ratio came to 0.57 at fractured sample after impact–fatigue loading (Fig. 8). It should be taking into account that this sample subjected to 422-repeated impacts. Along the experiments it was clearly observed that there was a plastic deformation occurred during the tests. This may causes small shifting of neutral axis of the materials. In Fig. 8 it is possible to see the original neutral axis, which was formed after first impact (indicated by arrows). It should be noted that the compression strength of the material is lower than the tensile strengths. The neutral axis symmetrically divides the cross-sections of the materials at the beginning of the experiments. That means approximately equal tensile and compression regions.

Figures 9–13 illustrates the fractured samples after single impact, which fractured with the izod hammer with an impact energy of 2.87 J. It should be noted that, this samples weren't previously impacted.

Figure 9 shows the boundary layer of the fracture surface of sample in tensile region. It is investigated the fracture of a fibre bundle in the composite specimen

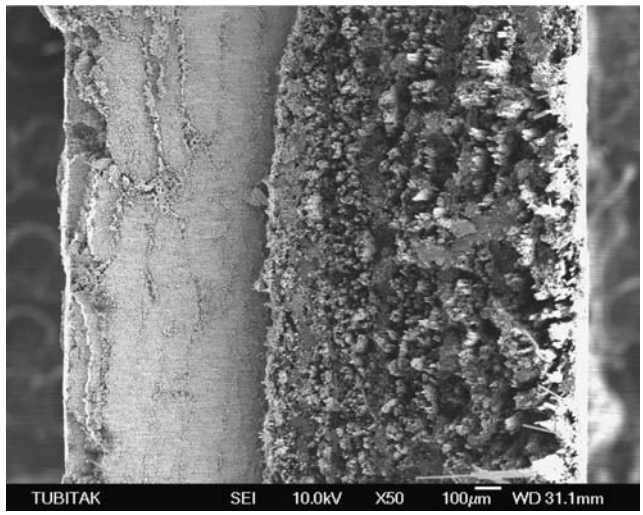

Fig. 7 Cross-section of sample fractured after single impact loading

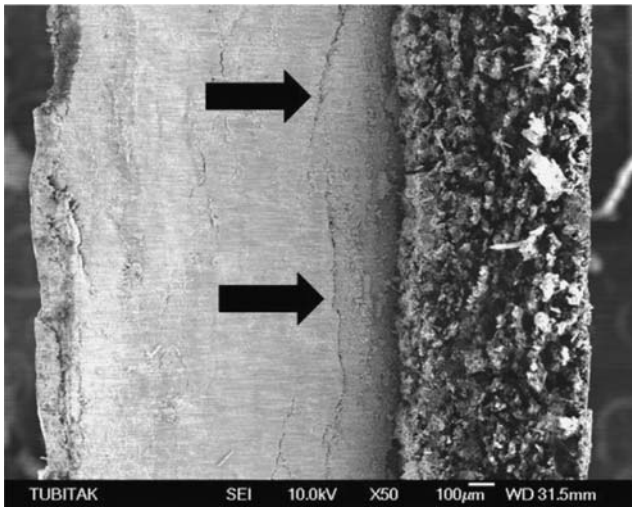

Fig. 8 Cross-section of sample fractured after 422 impact–fatigue loading

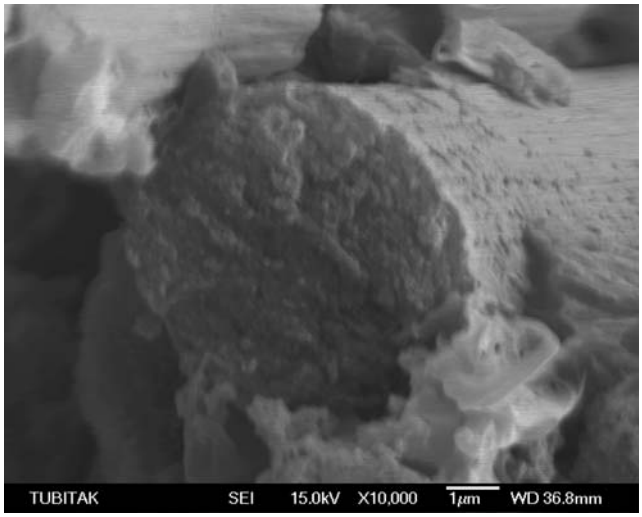

Fig. 10 Fractured carbon fibre surface at tensile zone

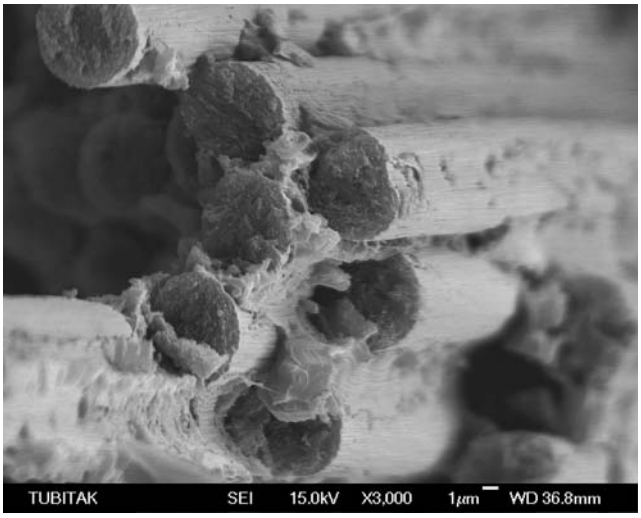

Fig. 9 Boundary layer of the fracture surface of sample at tensile zone

Fig. 11 Neutral axis image

with PEI matrix. These fibres seem to have very strong interfacial bond to the matrix. The high interfacial strength between the fibre and matrix leads eventually to extensive transverse fibre fracture on the back face of impact rather than pulling-out of fibres, matrix cracking, etc. As investigated by Roy [6] and Lee et al. [20] fibres fractured in a brittle manner without any indication of yield or flow. As a result of strong fibre-matrix interfacial bond strength the pull-out lengths shows very short stub of carbon fibre [19]. The fracture surface of the fibres is perpendicular to the fibre axis and has chevron markings. Figure 10 shows clearly the chevron markings on the surface of broken fibres. Chevron markings are particularly useful in assessing the direction of crack propagation and, by inference, the location of the crack origin [20]. As explained in ref. [22] crazing initiated at broken fibres. Darker areas on the image are evidence of topographical low points.

As illustrated in Fig. 11, there were many fibres having arbitrary angle on and nearby the neutral axis. It is easy to follow the neutral axis even by naked eye. The two different patterns meet near the neutral axis. As seen in Fig. 11, neutral axis behaves like a smooth boundary, or transition zone between the tensile and compression zones. It is possible to see some bended and fractured fibres as a result of bending at the tensile zone nearby the neutral axis. It can also be noted that this bended fibres has a tendency of fracture during the impact–fatigue loading. This was the reason for the neutral axis to move towards the tensile zone after

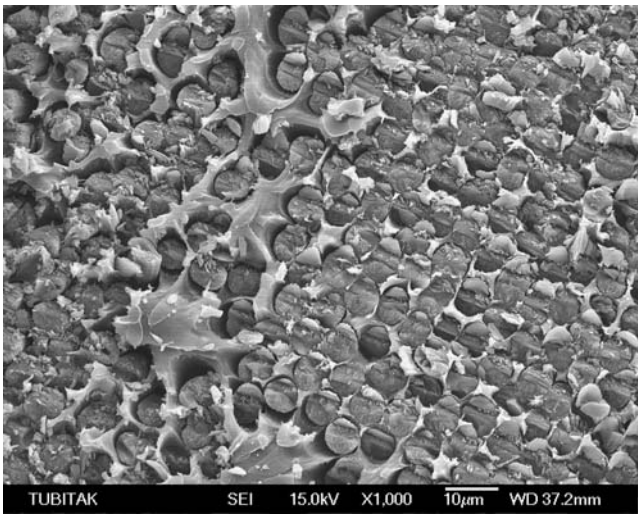

Fig. 12 Fracture surface of fibres in the compression zone

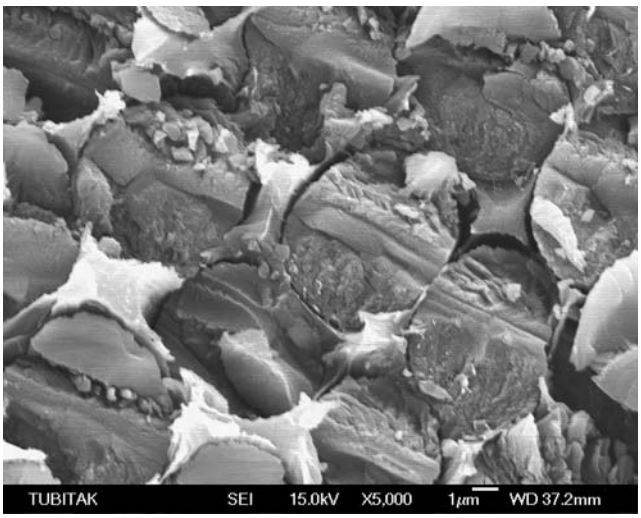

Fig. 13 Fibres at compression zone with a wrinkled morphology

impact–fatigue tests. There are some fibres, which were located very close to the neutral axis, shows both tensile and compression type fracture. Bending induces tensile and compressive stresses across the fibre. The flexure of an initially straight fibre leads to nucleation of the shear deformation bands on the compressive side of the fibre. Carbon fibres are then fractured in the tensile region in a brittle manner, followed by shear failure in the compressive region.

In Figure 12, there is a wrinkled pattern on the fracture surface of all fibres (showing the shear breakage of the fibres) observed in the compression zone very similarly as reported in previous studies [6, 20]. In addition to shear-fractured fibres, small fibre fragments as a result of microbuckling and fractures of resin can be observed in Fig. 12. Fractures of the polyetherimide matrix are formed in irregular patterns including the matrix fragments of 0.5–5 μm size. As explained by Sohn et al. [21] the extensive fragmentation of the matrix can be attributed to compression and shear fracture from the impact loading and can be contrasted with the matrix fracture occurring under quasi-static loading conditions. In addition to shear fractured fibres, as reported by Lee et al. [20] cracking through the fibres is also observed. Figure 13 also shows the fibres at compression zone at higher magnification. The shear bands on the fibres also indicate the crack propagation direction [22].

Figures 14 and 15 illustrates the fracture surfaces of samples, which were fractured at 422nd impact with the izod hammer, which has an impact energy of 0.35 J. It should be remembered that, this samples had no crack initiation at first impact as seen in Fig. 2d.

As seen in Fig. 14, similar to single-impact fractured samples; fibres were fractured in a brittle manner without showing any indication of yield or flow at impact–fatigue loading. Fracture surface of the fibres was perpendicular to the fibre axis and has a chevron markings like single-impact fractured sample. On the other hand a remarkable change was observed especially at the boundary of the tensile zone with lots of pulled-out fibre. Cycling impact loading causes plastic deformations at the matrix. As a result of repeated impacts relative shear loadings between the fibre surface and matrix, a cavity-like plastically deformed hollow holes occurred around the fibres. These holes may widen by the results of repeated impacts. By tearing and coalescence of this failures transforms to cracking through the fibres.

Figure 15 shows a special fracture morphology, which exhibits characteristic of impact–fatigue behaviour,

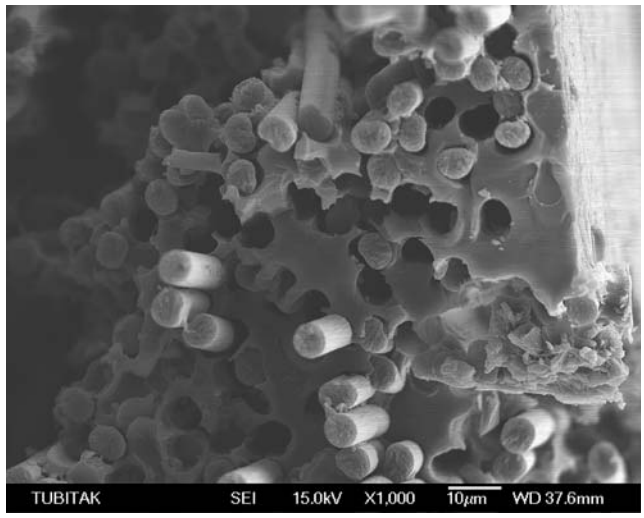

Fig. 14 Fractured fibres at the tensile zone as a result of impact–fatigue loading

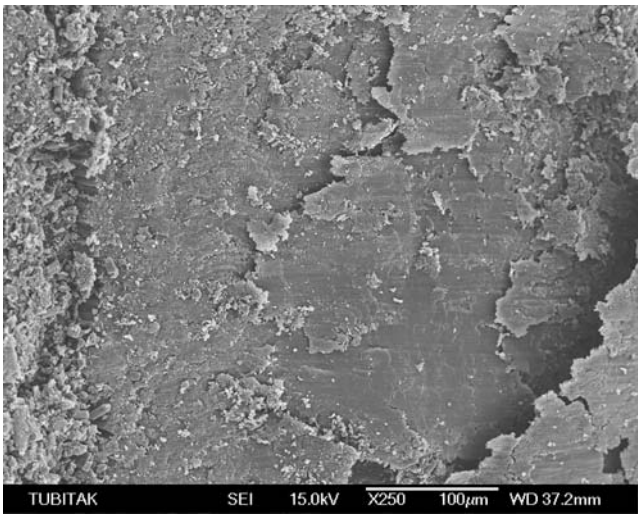

Fig. 15 Compression zone of fractured samples as a result of fatigue–impact loading

which was also explained in previous studies [6, 20, 22] The fibre-matrix debonding process is a progressive mechanism, that initiates from fibre breaks, and grows in mode II in the same direction as that of the fibres and applied load. During the impact–fatigue loading and crack propagating, there was a slippage occurred between the surfaces of the cracks. As a result of local shear yielding (By means of this slippage) of the matrix, thin layer of PEI resin (including matrix fragments) covers the whole compression region. This PEI layer includes also the carbon fibre fragments due to micro buckling and shears deformations.

Conclusion

The impact properties and the effects of the pre-impaction on the final impact properties of carbon fibre reinforced PEI composites were studied and it was observed that as expected the impact energy of the hammer and the number of pre-impacts were main parameters. Decrease in impact energy resulted with an increase in the number of impacts to failure. The final impact values of the composites were decreased remarkably after the pre-impacts with a impact energy at more than 0.39 J. On the other hand although there was no crack formation at 0.35 J, as a result of impact–fatigue loading deformations at sub surface were coalescence and crack formations occurred in time and propagates.

Pre-impacted samples showed different fracture behaviour and morphology compare to single fractured sample without pre-impacts. The neutral axis was moved towards tensile zone with increasing number of pre-impacts.

References

1. Sohn MS, Hu XZ (1995) Composites 26(12):849
2. Papanicolaou GC, Stavropoulus CD (1995) Composites 26(7):517
3. Novak RC, Decrecent MA (1972) In: Impact behaviour of unidirectional composites. ASTM STP 497, American Society for Testing and Materials, New York, pp 311
4. Caprino G (1983) J Mater Sci 18(8):2269
5. Caprino G (1985) J Compos Mater 18:508
6. Roy R, Sarkar BK, Bose NR (2001) Composites: Part A 32:871
7. Lal KM (1986) J Reinf Plast Compos 2:226
8. Cantwell WJ, Curtis PT, Morton J (1984) Int J Fatigue 6(2):113
9. Wyrick DA, Adams DF (1988) J Compos Mater 22:749
10. Jang BP, Kowbel W, Jang BZ (1992) Compos. Sci. Technol 44:107
11. Ho KC, Hwang JR, Doong JL (1997) J Reinf Plast Compos 16(10):903
12. Yang P, Liu Y, Xu F (1998) J Mater Eng Perform 7(5):677
13. Shin HS, Maekawa I (1997) Damage and failure interfaces. Balkema, Rotterdam, pp 343
14. Lhymn C (1985) J Mater Sci Lett 4:1221
15. Lhymn C (1985) J Mater Sci Lett 4:1429
16. Rotem A (1988) J Compos Technol Res Summer 74
17. Tamuzs VP, Kuksenco VS (1981) In: Fracture micromechanics of polymer materials The Hague, Amsterdam
18. Jang BP, Huang CT, Hsieh CY, Kowbel W, Jang BZ (1991) J Compos Mater 25:1171
19. Friedrich K, Karger Kocsis J (1989) In: Fractography and failure mechanisms of polymers and composites. Elsevier Applied Science, Banking, p 437
20. Lee CS, Hwang W, Park HC, Han KS (1999) Compos. Sci. Technol. 59:1789
21. Sohn MS, Hu XZ, Kim JK, Walker L (2000) Composites: Part B 31:681
22. Gdoutos EE, Pilakoutas K, Rodopoulos CA (2000) Failure analysis of industrial composite materials, McGraw-Hill Inc, New York